THE JOURNAL OF PHYSICAL CHEMISTRY C
A JOURNAL OF THE AMERICAN CHEMICAL SOCIETY

pubs.acs.org/JPCC

Article

Transient Energy-Resolved Photoluminescence Study of Excitons and Free Carriers on $FAPbBr_3$ and $FAPbBr_3/SnO_2$ Interfaces

Xinjian Geng, Yawen Liu, Xianshao Zou, Erik M. J. Johansson, and Jacinto Sá*

Cite This: *J. Phys. Chem. C* 2023, 127, 3085−3092

Read Online

ACCESS | Metrics & More | Article Recommendations | Supporting Information

ABSTRACT: Lead bromide perovskites have a larger band gap and are significantly more stable than their iodine counterparts, offering the perspective for higher voltage, tandem photovoltaics exceeding the Shockley−Queisser limit, and shorter time to deployment of photovoltaics. However, their efficiencies still need to be rivaling the iodine ones. Herein, the photophysics of $FAPbBr_3$ and the ones behind electron transfer from $FAPbBr_3$ to SnO_2, one of the most effective electron transporting materials (ETMs), are reported. Time- and energy-resolved photoluminescence studies revealed the existence of two emitting states in the perovskite, which were assigned to bounded excitons and free carriers. SnO_2 extracted electrons from excitons and free carriers, with a selectivity related to the SnO_2 surface treatment. This new insight helps explain SnO_2's unique qualities as an ETM to produce photovoltaics with reduced voltage losses. Furthermore, this study illustrates the importance of performing time- and energy-resolved photoluminescence to capture the intricacies of the photophysical process.

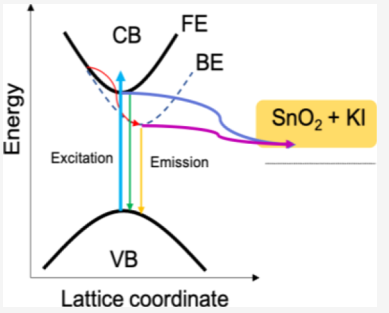

Downloaded via UPPSALA UNIV on May 10, 2023 at 08:59:54 (UTC).
See https://pubs.acs.org/sharingguidelines for options on how to legitimately share published articles.

INTRODUCTION

Energy use is ubiquitous in almost every human activity. The rising global temperatures threaten to trigger severe climate change events that will affect everyone and everything. Mitigation strategies such as increasing coastal defenses, reducing soil erosion, and executing reforestation projects are being realized in the areas already at risk. The consensus is that to stop the worse from happening, humans need to meet their energy demands using renewable energy instead of fossil fuels. There is a consensus that electrifying all human activities that can be electrified enables the direct use of wind- and solar-generated power and reduces air pollution. Therefore, there is a significant research effort to improve and develop photovoltaics and wind-turbine technologies that can produce the necessary electricity that reached ca. 26,000 TWh in 2020 and is forecast to grow annually between 2.5 and 4%.[1]

Lead halide perovskites are the most researched topic concerning a novel photovoltaic technology. In 2009, Kojima et al.[2] introduced this class of materials as potential active materials for photovoltaics, reporting a device with efficiencies of around 9%. Based on previous photovoltaic technologies' progress, people could only predict perovskite photovoltaics' meteoric upsurge in performance, which exceeds 25% today.[3−5] Issues related to stability and the use of lead need to be addressed for their commercial deployment, but progress is being made by introducing polymeric interlayers,[6−8] engineering material dimensionality,[9,10] and using tin as an alternative to lead.[11,12]

Iodine-based perovskite systems dominate the ranking of record photovoltaic cells. Recently, lead bromide perovskites gained great attention[13−19] as an exciting candidate for the top cell of tandem devices, benefiting from its high band gap (around 2.3 eV), high V_{oc}, and good chemical stability in ambient air.[20−22]

Transient photoluminescence (TRPL) studies are widely used to follow charge recombination decay that provides valuable insights into the charge lifetime and quenching efficiency, which can be correlated with the photovoltaic performance. This is commonly done by single-photon counting, which solely addresses the time component.[23,24] In this work, we report a time- and energy-resolved TRPL study utilizing a streak camera with femtosecond pulse excitation.[25−29] The results reveal the existence of two emitting states from $FAPbBr_3$, which are harnessed differently by the electron transporting layer (ETL) (SnO_2) when its surface is treated with KI.

METHODS

Preparation of Perovskite Samples. A colloidal dispersion of tin oxide (15% in H_2O, Alfa Aesar) was diluted with deionized water, and the volume ratio of water to SnO_2 is 4:1. Potassium iodide (KI, 1.2 mg/mL) was added into the diluted SnO_2 dispersion for preparing the SnO_2 + KI substrate. The SnO_2 dispersion was then deposited on the glass slide by

Received: November 11, 2022
Revised: January 19, 2023
Published: February 2, 2023

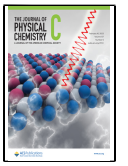

ACS Publications

© 2023 The Authors. Published by American Chemical Society

spin coating at 3000 rpm for 30 s. The film was annealed at 150 °C for 30 min followed by the UV/ozone treatment for 20 min.

1.1 M $PbBr_2$ was prepared in a mixture of dimethylformamide and dimethyl sulfoxide with a volume ratio of 9:1 and stirred at 60 °C overnight. The first step was spin-coating the $PbBr_2$ solution on different substrates at 1500 rpm for 20 s and 5000 rpm for 30 s. Then, the films were annealed at 70 °C for 1 min. The second step was depositing a FABr (65 mg/mL in methanol) solution over the $PbBr_2$ films (2000 rpm, 30 s), and the films were annealed at 140 °C for 25 min in the air.

Characterization of Films. UV−vis absorption was determined by a Cary 5000 spectrophotometer. Steady-state photoluminescence (PL) was conducted on an Edinburgh FS5 spectrofluorometer.

Time-resolved PL was performed on a streak camera detection system. The 515 nm excitation wavelength was generated from the fundamental 1030 nm laser (200 kHz, Jasper 10, Fluence). The pump power was adjusted to 1 mW by a graduated neutral density filter, and the angle of the excitation beam hitting the perovskite side was 45°. After being transmitted through a long-pass filter, PL emission was detected by a streak camera (C5680 + M5675, Hamamatsu).

RESULTS AND DISCUSSION

For this study, we prepared films consisting of the formamidinium bromide perovskite ($FAPbBr_3$) on thin glass slides with and without a coating of SnO_2. Details of material synthesis and film preparation can be found in the Supporting Information (SI). The systems were extensively characterized in a previous publication;[30] thus, the focus of this contribution is the optical part. $FAPbBr_3$ on glass was used as a reference sample to depict the underlying photophysics without charge extraction. Figure 1a shows the UV−vis absorbance and PL of this film. The absorbance is dominated by a sharp absorption edge starting at ca. 545 nm and an excitonic peak at 529 nm. The emission overlaps the absorption edge and has a peak at 546 nm.

Deconvolution of the PL with a single component did not produce a good fit with R^2 = 0.972 (see Supporting Information Figure S1). Figure 1b shows the deconvolution considering two components that yielded an R^2 = 0.999. Since $FAPbBr_3$ is expected to be a pure orthorhombic phase,[24,30,31] one can exclude the possibility of the second peak being associated with the mixture of crystalline phases. This also supported the X-ray diffraction pattern presented in Figure S5, consistent with previously published diffractograms.[32,33] Another possibility for the doublet is that it relates to defect-related trap states.[25] However, the overlapping nature of absorbance and emission features and the relatively narrow PL global peak suggest otherwise. A more plausible explanation is that emissions relate to free carriers (higher energy PL peak) and bounded excitons (lower energy PL peak), as suggested recently for the methylammonium bromide perovskite ($MAPbBr_3$).[31] This establishes the exciton energy at about 60 meV (estimated from the exciton peak energy 2.343 eV minus the free-carrier emission energy ca. 2.283 eV,[34] see Supporting Information Table S1), consistent with what was previously reported[35,36] and higher than its iodine perovskite counterpart.[37,38]

To test the hypothesis, a time- and energy-resolved TRPL study utilizing a streak camera with femtosecond pulse excitation measurements was performed. If the hypothesis is

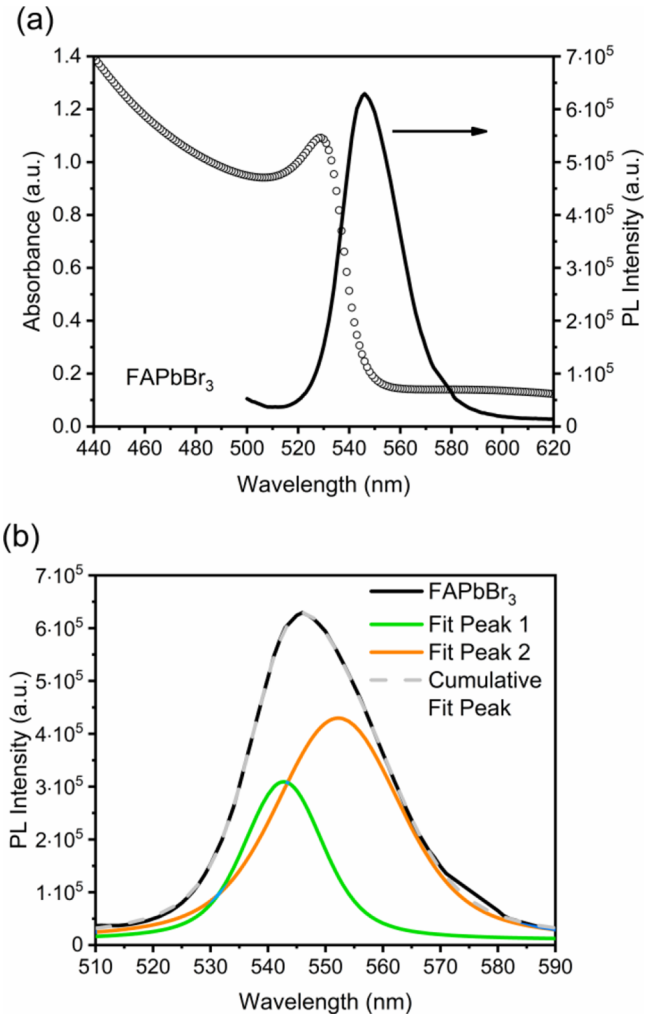

Figure 1. Steady-state UV−vis absorbance and emission upon excitation at 470 nm of $FAPbBr_3$. (a) Overlapped signal of absorbance and emission and (b) deconvolution of the emission signal.

correct, one should expect different rising components for each species and different times and models for the decays. The laser pulse was fixed at 515 nm (above the band gap energy), and its duration was around 300 fs. Note that the novelty of the manuscript is to follow what happened in the early times (inaccessible to techniques, such as time-correlated single-photon counting), where excitons and free carriers coexist and thus permit assessing whether carriers can be extracted directly from an exciton, which is particularly relevant in this system since it has an exciton energy higher than the room temperature. Later, carriers are injected as free or trapped carriers but never as excitons because they have already recombined or broken into free carriers. It is worth mentioning that perovskites are known to have long-lived and injectable states (up to 200 μs) that have been thoroughly characterized by time-correlated single-photon counting.[39]

To establish the optimal laser fluence that ensures a good signal-to-noise ratio and coexistence of excitons and free carriers, TPRL signal power dependence measurements were performed (Figure 2). A linear fit of the data shows that above 10 W/cm^2, the slope is larger than unity (i.e., 1.5), consisting of co-mingling of excitons and free-carrier recombination.[40,41] Below 10 W/cm^2, the slope is closer to 2, consistent with PL related primarily to free-carrier recombination. Note that PL

https://doi.org/10.1021/acs.jpcc.2c07931
J. Phys. Chem. C 2023, 127, 3085−3092

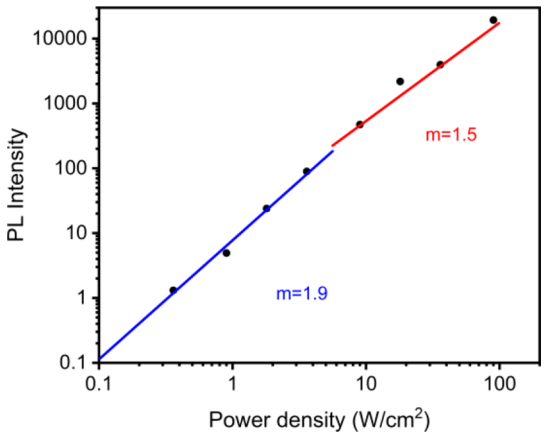

Figure 2. Power dependence of the accumulated TRPL signal of $FAPbBr_3$ on glass upon excitation at 515 nm with a 300 fs laser pulse and accumulated for 1000 ps.

related primarily to exciton recombination would yield a unity slope. Therefore, the optimal pulse energy was established to be 18 W/cm^2, ensuring a good signal-to-noise ratio while staying within the constant ratio of the squared population of free carriers over that of the excitons according to the Saha equation (see Supporting Information Figure S2).[42,43] The Saha equation correlates the ratio of free carriers and excitons to the excitation density in a hot electron−hole plasma.[44,45]

The TPRL results are summarized in Figure 3 and Supporting Information Tables S1 and S2. Note that small shifts around 10−20 nm are expected when comparing transient with steady-state PL data. The fitting of the global TRPL after 1000 ps provided more substantial evidence for a two-peak component (Figure 3a and Supporting Information Table S1) with a similar peak ratio as the steady-state data.

The lower energy component kinetic trace was extracted between 565 and 575 nm to reduce the overlap with the high-energy component. The kinetic trace had a rising edge of 37 ps and a single exponential decay with τ = 520 ± 12 ps (Figure 3b and Supporting Information Table S2). The rising edge relates to the exciton lifetime. Lifetimes in tens to hundreds of picoseconds suggest that multiple excitons are being formed since single excitons have lifetimes in tens of nanoseconds.[46] The extracted decay is consistent with what is expected for bounded exciton recombination since they are formed instantaneously to our time resolution and decay by simple electron−hole annihilation.

The higher energy peak is centered at 528 nm and shows considerable overlap with the exciton component. Fittings across the width of the band were performed to establish the energy range where there is a minimal contribution from the low-energy band and the signal-to-noise ratio is still good. While in the accumulated PL spectrum in Figure 3a, this seems unachievable, one can ensure that in the time domain, this energy range is easier to identify, and, in the present case, it was found to be between 520 and 530 nm. Please check the Supporting Information section explanation of the TRPL peak deconvolution for further substantiation of our claim.

The kinetic trace extracted from the 520−530 nm region was fitted with a rising component of 55 ps and a bi-exponential decay, namely τ_1 = 120 ± 11 ps (50%) and τ_2 = 1222 ± 69 ps (50%) (Figure 3c and Supporting Information Table S2). The rising component is more significant than the instrument response function (IRF) (ca. 25 ps), meaning this

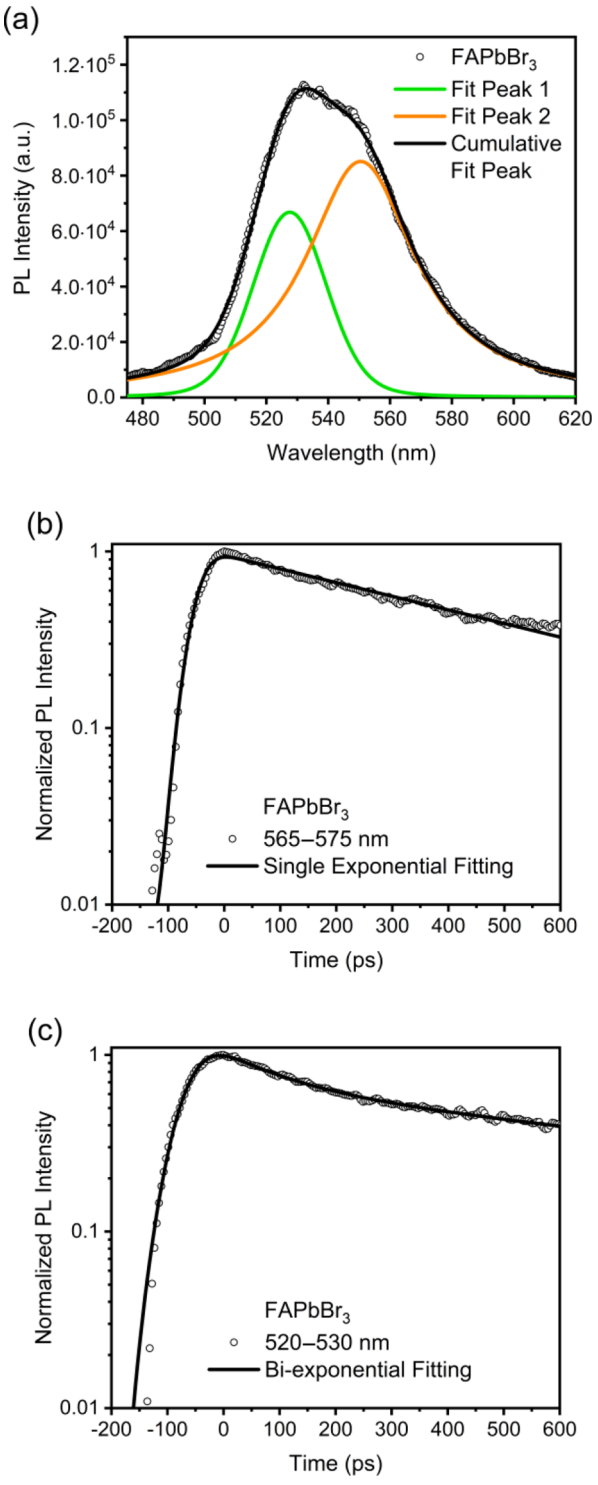

Figure 3. TRPL of $FAPbBr_3$ on glass upon excitation at 515 nm with a 300 fs laser pulse and a photon energy of 18 W/cm^2. (a) Deconvolution of the accumulated PL signal after 1000 ps; (b) kinetic decay of the signal extracted between 565 and 575 nm (bounded excitons); and (c) kinetic decay of the signal extracted between 520 and 530 nm (free carriers). Note that TRPL fittings are shown till 600 ps but performed over a 1 ns time range, ensuring at least 60−70% signal decay.

is the associated time for the emitting component to reach the maximum number of emitters before its decay, i.e., the time associated with the cooling down of charges and filling the

https://doi.org/10.1021/acs.jpcc.2c07931
J. Phys. Chem. C 2023, 127, 3085−3092

emitting state. High-quality perovskite films display larger diffusion lengths; consequently, they will take longer to fill the emitting states.[47] According to our hypothesis, the higher energy component relates to free carriers, which must follow a bimolecular decay mechanism consistent with the observation.[48]

The data are then consistent with the proposed hypothesis. Figure 4 presents a Jablonski-type diagram summarizing the photophysics phenomena. Upon band gap excitation with photons above the energy threshold (blue arrow), the excited carriers form bounded excitons or break into free carriers within 37 ps. The bounded excitons reach their maximum population instantaneously to our temporal resolution, and their radiative decay (orange arrow) could be fitted with a single exponential decay. The free carriers take about 55 ps to reach their maximum. The kinetic trace of the radiative decay (green arrow) follows a bi-exponential model as expected for bimolecular recombination.

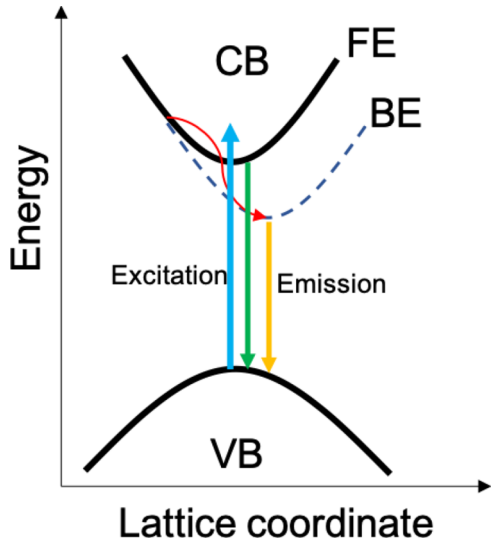

Figure 4. Jablonski-type diagram summarizing photophysics of $FAPbBr_3$. CB, conduction band; VB, valence band; FE, free electrons; and BE, bounded excitons.

An n−i−p structure is a common perovskite photovoltaic architecture, and SnO_2 is among the best-performing ETL materials,[15,19,30,49] with an added benefit that it can be processed from solution at a low temperature. Thus, studying the material's ability to extract charge from the two identified states is pertinent. Figure 5a shows the UV−vis absorbance and PL of $FAPbBr_3$ deposited on SnO_2 on a glass film. As with the case of $FAPbBr_3$ on glass, the emission is narrow and overlaps nicely with the absorption edge, which has an identical position as $FAPbBr_3$ on glass. In this case, deconvolution of the PL signal could be done with a single component, yielding an $R^2 = 0.998$ (Figure 5b and Supporting Information Table S2). Note that the perceived small shoulder at lower energies is believed to be an artifact from a source reflection that we removed from the spectrum. However, we cannot rule out small amounts of an intermediate crystal phase.[33] Yet, this signal was not visible in the TPRL data.

TRPL confirmed the observation of an accumulated PL signal after 1000 ps (Figure 6a). Also, the best fit required only a rising edge and a single exponential decay (Figure 6b). This, allied to the emission centered around 555 nm, suggests that

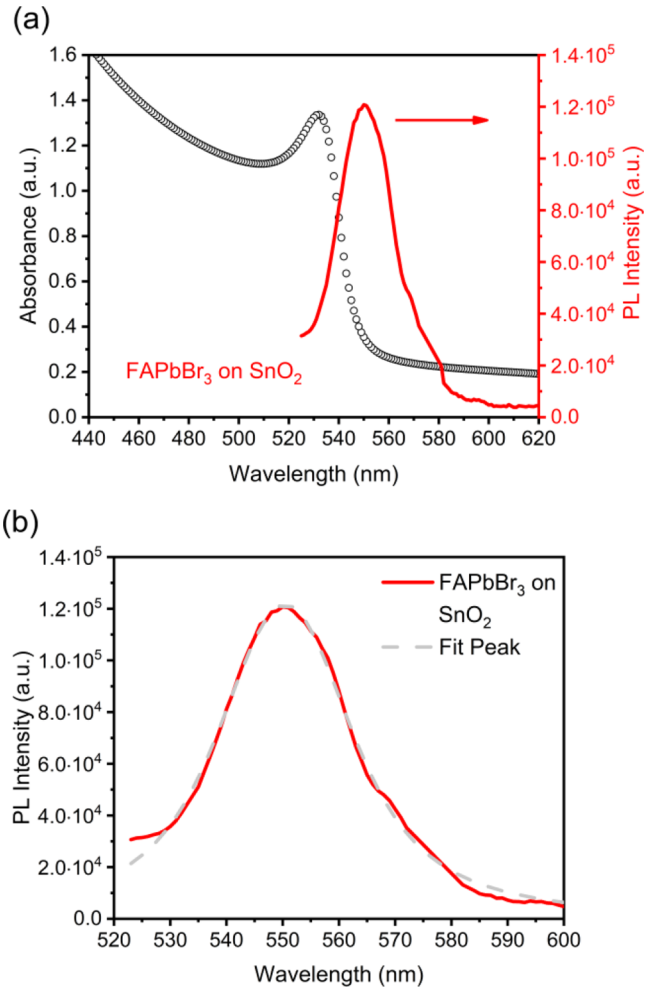

Figure 5. Steady-state UV−vis absorbance and emission upon excitation at 470 nm of $FAPbBr_3$ on SnO_2. (a) Overlapped signal of absorbance and emission and (b) deconvolution of the emission signal.

the signal is related to bounded excitons. This finding advocates a preference for electron extraction from the free-carrier population, as depicted in the Jablonski diagram in Figure 7, leading to the suppression of this emission channel. Fitting of the emission could be done with a single exponential (τ = 1468 ± 48 ps) and a rising edge with 34 ps, consistent with bounded exciton emission (Figure 6b and Supporting Information Table S2). The ultrafast rising edge confirms once more the creation of multiple excitons.[46]

The SnO_2 ETL often exhibits defect-related issues associated with the perovskite/SnO_2 interface. These defect states can be passivated, and commonly, potassium ions are used.[26,50−53] It has been found that the potassium treatment shifts the conduction band minimum and Fermi energy of SnO_2 to higher energy, resulting in a better conduction band alignment at perovskite/SnO_2.[54,55]

There is also a possibility that K ions diffused into the bulk perovskite, enlarged the grain size, and passivated the grain boundaries.[55] Still, our measurement is less sensitive to that compared to changes in interface charge extraction. Due to the prevalence of such a treatment to achieve high-performing photovoltaic devices, it is relevant to study if this surface treatment has any effect from where the electrons are extracted.

https://doi.org/10.1021/acs.jpcc.2c07931
J. Phys. Chem. C 2023, 127, 3085−3092

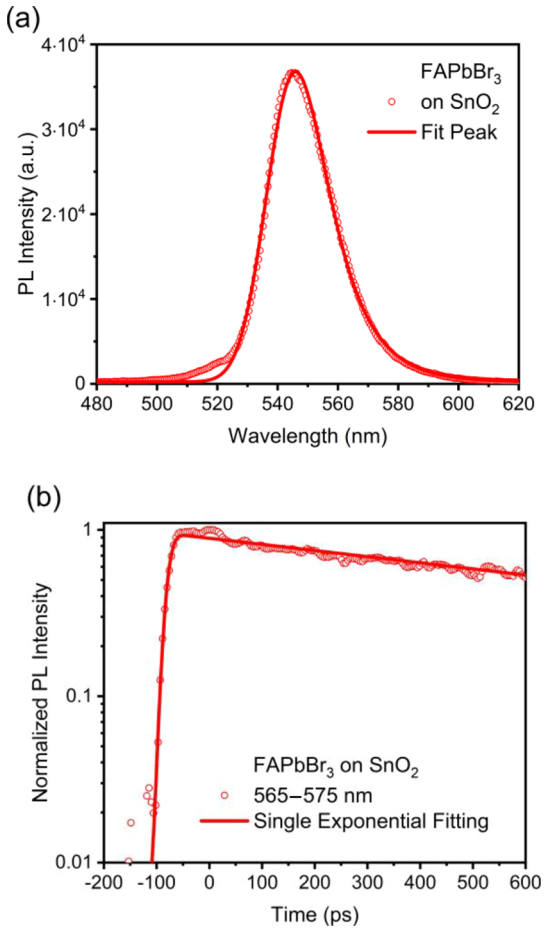

Figure 6. TRPL of $FAPbBr_3$ on SnO_2 upon excitation at 515 nm with a 300 fs laser pulse and a photon energy of 18 W/cm^2. (a) Deconvolution of the accumulated PL signal after 1000 ps and (b) kinetic decay of the signal extracted between 565 and 575 nm (bounded excitons). Note that TRPL fittings are shown till 600 ps but performed over a 1 ns time range, ensuring at least 60−70% signal decay.

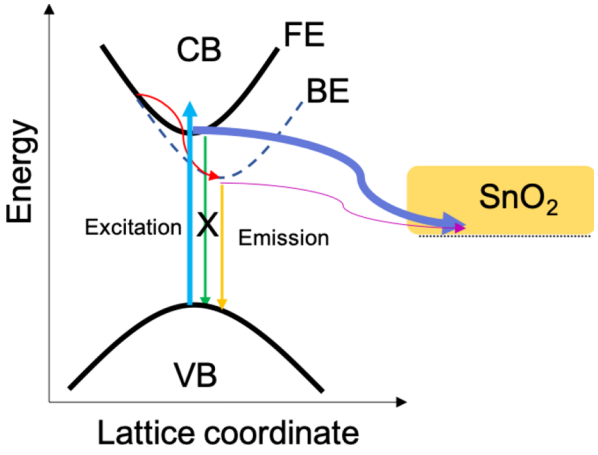

Figure 7. Jablonski-type diagram summarizing photophysics of $FAPbBr_3$ on SnO_2. CB, conduction band; VB, valence band; FE, free electrons; and BE, bounded excitons.

Figure 8a shows the UV−vis absorbance and PL of $FAPbBr_3$ deposited on SnO_2 treated with KI after deposition on glass. Similar to the previous case, the emission is narrow and

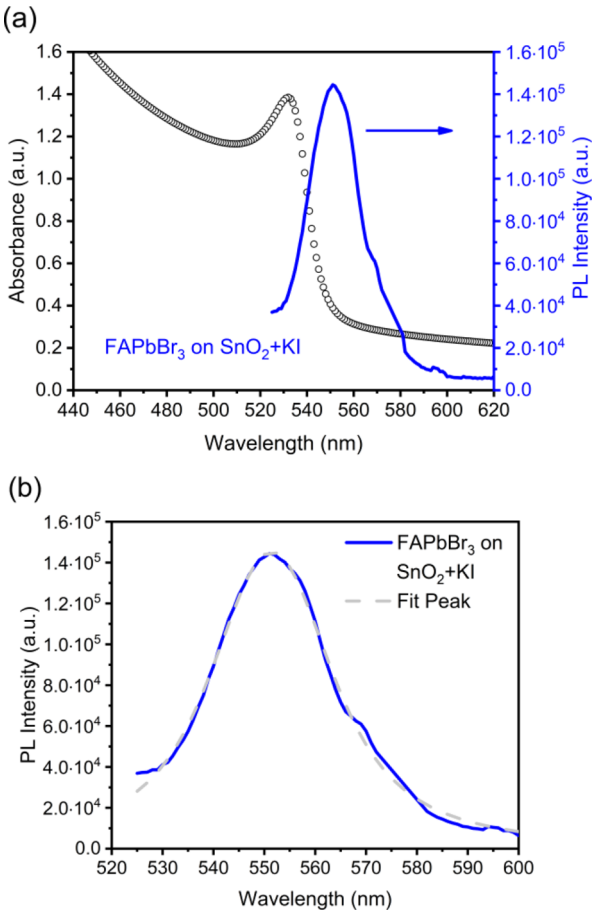

Figure 8. Steady-state UV−vis absorbance and emission upon excitation at 470 nm of $FAPbBr_3$ on SnO_2 treated with KI. (a) Overlapped signal of absorbance and emission and (b) deconvolution of the emission signal.

overlaps nicely with the absorption edge, which is identical to $FAPbBr_3$ on glass. Deconvolution of the PL signal could be done with a single component with an $R^2 = 0.997$ (Figure 8b).

The fitting of the global TRPL after 1000 ps required two components (Figure 9a), similar to what was observed with the perovskite on glass but contrasting the result obtained for the perovskite on untreated SnO_2. It is worth noticing that the peak ratio of the accumulated TRPL emission after 1000 ps is similar to the steady-state ratio observed on the perovskite alone.

Analysis of the kinetic traces (Figure 9b,c) revealed that the higher energy component has a rising edge with about 48 ps, and its decay requires a bi-exponential model to be fitted with $\tau_1 = 123 \pm 19$ ps (38%) and $\tau_2 = 1883 \pm 140$ ps (62%) (Figure 8c). This is once more consistent with free-carrier emission. The component at lower energy was fitted with a single exponential decay ($\tau = 1168 \pm 36$ ps) and a rising function of 16 ps that is lower than our IRF (Figure 9b, again consistent with bounded exciton emission (Supporting Information Table S2).

The results suggest that the potassium treatment that induces an upward shift of the conduction band maximum and Fermi energy of SnO_2 significantly changed the electron extraction ratio of the bounded excitons and the free electrons (Figure 10), with potential implications for the photovoltaic efficiency, which are beyond the focus of this study. It is,

https://doi.org/10.1021/acs.jpcc.2c07931
J. Phys. Chem. C 2023, 127, 3085−3092

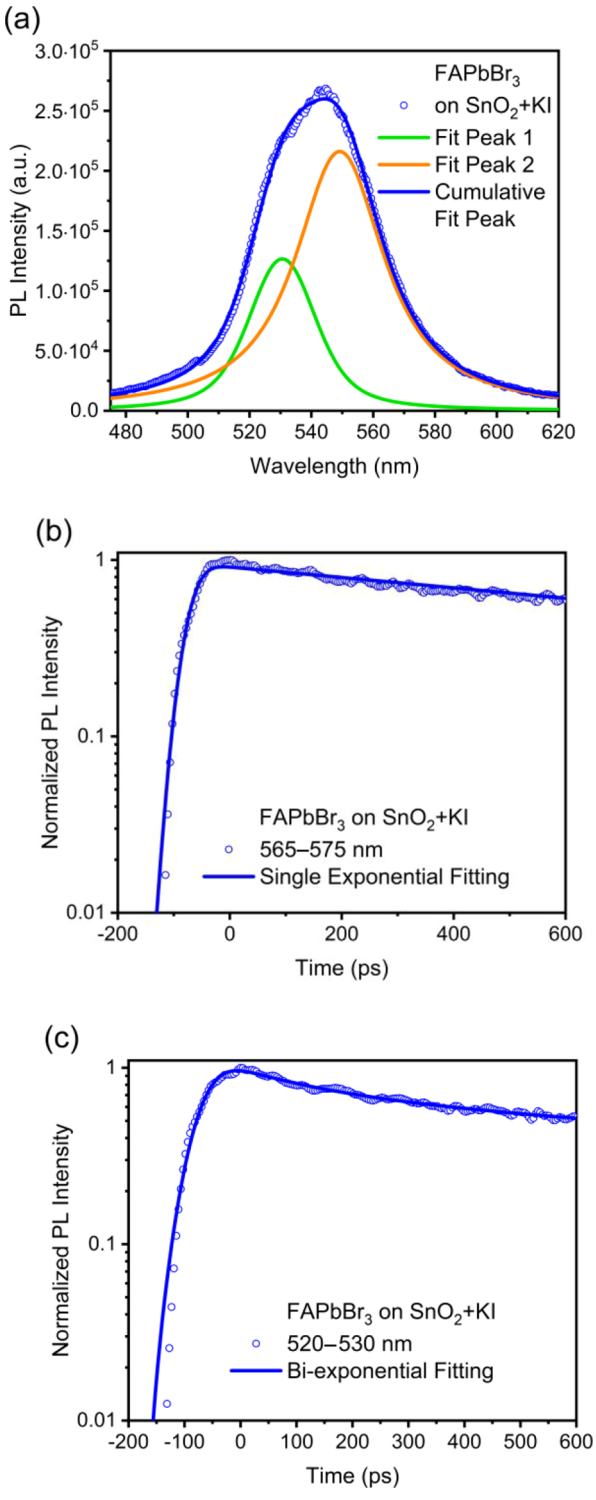

Figure 9. TRPL of $FAPbBr_3$ on SnO_2 treated with KI upon excitation at 515 nm with a 300 fs laser pulse and a photon energy of 18 W/cm^2. (a) Deconvolution of the accumulated PL signal after 1000 ps; (b) kinetic decay of the signal extracted between 565 and 575 nm (bounded excitons); and (c) kinetic decay of the signal extracted between 520 and 530 nm (free carriers). Note that TRPL fittings are shown till 600 ps but performed over a 1 ns time range, ensuring at least 60−70% signal decay.

however, important to stress that efficient electron extraction directly from excitons requires good electronic coupling and band alignment,[56] which motivates potassium-treated SnO_2 as the ideal ETL for this particular perovskite.

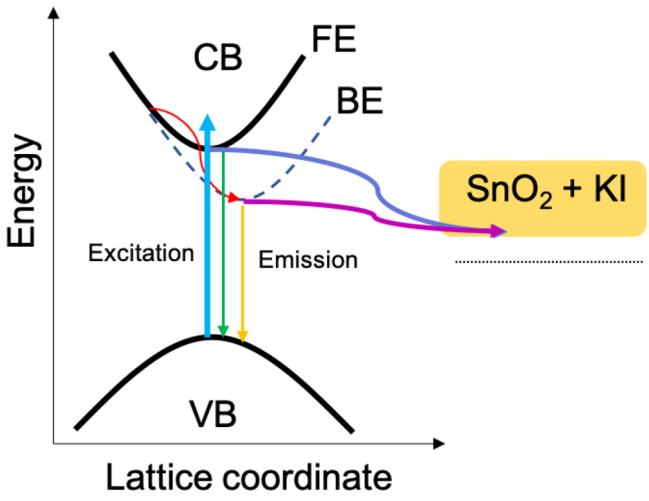

Figure 10. Jablonski-type diagram summarizing photophysics of $FAPbBr_3$ on KI-treated SnO_2. CB, conduction band; VB, valence band; FE, free electrons; and BE, bounded excitons.

CONCLUSIONS

In conclusion, lead bromide perovskites are promising for tandem solar cells. This contribution studied the photophysics of $FAPbBr_3$ and $FAPbBr_3/SnO_2$ interfaces. TRPL revealed the existence of two emitting states associated with free carriers and bounded excitons. SnO_2, a popular ETL, preferentially harvests electrons from the free-carrier population. However, when its surface is treated with potassium, the electrons are extracted from both states with a similar apparent probability, directly affecting overall photovoltaic efficiencies. Direct extraction of electrons from excitons requires good electronic coupling and band alignment at the interface, motivating the use of potassium-treated SnO_2 as an ETL, at least for this class of perovskites.

ASSOCIATED CONTENT

Supporting Information

The Supporting Information is available free of charge at https://pubs.acs.org/doi/10.1021/acs.jpcc.2c07931.

Experimental work and additional characterization data, including power-dependent PL and XRD of the perovskite and UPS of the SnO_2 films (PDF)

AUTHOR INFORMATION

Corresponding Author

Jacinto Sá − *Physical Chemistry Division, Department of Chemistry - Angstrom Laboratory, Uppsala University, Uppsala 751 20, Sweden; Institute of Physical Chemistry, Polish Academy of Sciences, Warsaw 01-224, Poland;* orcid.org/0000-0003-2124-9510; Email: jacinto.sa@kemi.uu.se

Authors

Xinjian Geng − *Physical Chemistry Division, Department of Chemistry - Angstrom Laboratory, Uppsala University, Uppsala 751 20, Sweden*

https://doi.org/10.1021/acs.jpcc.2c07931
J. Phys. Chem. C 2023, 127, 3085−3092

Yawen Liu − *Physical Chemistry Division, Department of Chemistry - Angstrom Laboratory, Uppsala University, Uppsala 751 20, Sweden*

Xianshao Zou − *Physical Chemistry Division, Department of Chemistry - Angstrom Laboratory, Uppsala University, Uppsala 751 20, Sweden;* orcid.org/0000-0002-9459-3147

Erik M. J. Johansson − *Physical Chemistry Division, Department of Chemistry - Angstrom Laboratory, Uppsala University, Uppsala 751 20, Sweden;* orcid.org/0000-0001-9358-8277

Complete contact information is available at: https://pubs.acs.org/10.1021/acs.jpcc.2c07931

Author Contributions

All the authors participated in the planning of the study. X.G. and Y.L. synthesized and prepared the samples and films. X.G. performed all the standard and the transient characterization, the latter with the help of X.Z. The data were analyzed and curated by X.G. J.S. drafted the manuscript with inputs from all the authors. X.G. prepared all the figures and tables. All the authors contributed to the final version of the manuscript and approved its submission.

Notes

The authors declare no competing financial interest.

■ ACKNOWLEDGMENTS

J.S. would like to acknowledge the Physical Chemistry unit of the Department of Chemistry-Angström, Uppsala University for the financial support for X.G.'s Ph.D. and the realization of this project. E.M.J.J. acknowledges the financial support from the Swedish Energy Agency, project number 46330-1, and the Physical Chemistry unit of the Department of Chemistry-Angström, Uppsala University.

■ REFERENCES

(1) https://www.aljazeera.com/news/2022/1/20/interactive-how-much-of-your-countrys-electricity-is-renewable-infographic, Accessed on November the 5th, 2022.

(2) Kojima, A.; Teshima, K.; Shirai, Y.; Miyasaka, T. Organometal Halide Perovskites as Visible-Light Sensitizers for Photovoltaic Cells. *J. Am. Chem. Soc.* **2009**, *131*, 6050−6051.

(3) Lee, M. M.; Teuscher, J.; Miyasaka, T.; Murakami, T. N.; Snaith, H. J. Efficient hybrid solar cells based on meso-superstructured organometal halide perovskites. *Science* **2012**, *338*, 643−647.

(4) Jung, H. S.; Park, N. G. Perovskite Solar Cells: From Materials to Devices. *Small* **2015**, *11*, 10−25.

(5) https://www.nrel.gov/pv/cell-efficiency.html, Accessed on November the 5th, 2022.

(6) Zuo, L.; Guo, H.; deQuilettes, D. W.; Jariwala, S.; De Marco, N.; Dong, S.; DeBlock, R.; Ginger, D. S.; Dunn, B.; Wang, M.; et al. Polymer-modified halide perovskite films for efficient and stable planar heterojunction solar cells. *Sci. Adv.* **2017**, *3*, No. e1700106.

(7) Yavari, M.; Mazloum-Ardakani, M.; Gholipour, S.; Tavakoli, M. M.; Taghavinia, N.; Hagfeldt, A.; Tress, W. Reducing Surface Recombination by a Poly(4-vinylpyridine) Interlayer in Perovskite Solar Cells with High Open-Circuit Voltage and Efficiency. *ACS Omega* **2018**, *3*, 5038−5043.

(8) Zhang, M.; Wu, F.; Chi, D.; Shi, K.; Huang, S. High-efficiency perovskite solar cells with poly(vinylpyrrolidone)-doped SnO_2 as an electron transport layer. *Mater. Adv.* **2020**, *1*, 617−624.

(9) Lee, J.-W.; Dai, Z.; Han, T. H.; Choi, C.; Chang, S.-Y.; Lee, S.-J.; De Marco, N.; Zhao, H.; Sun, P.; Huang, Y.; et al. 2D perovskite stabilized phase-pure formamidinium perovskite solar cells. *Nat. Commun.* **2018**, *9*, 3021.

(10) Shao, M.; Bie, T.; Yang, L.; Gao, Y.; Jin, X.; He, F.; Zheng, N.; Yu, Y.; Zhang, X. Over 21% Efficiency Stable 2D Perovskite Solar Cells. *Adv. Mater.* **2022**, *34*, No. 2107211.

(11) Sun, N.; Gao, W.; Dong, H.; Liu, Y.; Liu, X.; Wu, Z.; Song, L.; Ran, C.; Chen, Y. Architecture of p-i-n Sn-Based Perovskite Solar Cells: Characteristics, Advances, and Perspectives. *ACS Energy Lett.* **2021**, *6*, 2863−2875.

(12) Gahlot, K.; de Graaf, S.; Duim, H.; Nedelcu, G.; Koushi, R. M.; Ahmadi, M.; Gavhane, D.; Lasorsa, A.; De Luca, E.; Rudolf, P.; et al. Structural Dynamics and Tunability for Colloidal Tin Halide Perovskite Nanostructures. *Adv. Mater.* **2022**, *34*, No. 2201353.

(13) Noh, J. H.; Im, S. H.; Heo, J. H.; Mandal, T. N.; Seok, S. I. Chemical Management for Colorful, Efficient, and Stable Inorganic−Organic Hybrid Nanostructured Solar Cells. *Nano Lett.* **2013**, *13*, 1764−1769.

(14) Edri, E.; Kirmayer, S.; Cahen, D.; Hodes, G. High Open-Circuit Voltage Solar Cells Based on Organic−Inorganic Lead Bromide Perovskite. *J. Phys. Chem. Lett.* **2013**, *4*, 897−902.

(15) Zhang, Y.; Liang, Y.; Wang, Y.; Guo, F.; Sun, L.; Xu, D. Planar $FAPbBr_3$ Solar Cells with Power Conversion Efficiency above 10%. *ACS Energy Lett.* **2018**, *3*, 1808−1814.

(16) Arora, N.; Dar, M. I.; Abdi-Jalebi, M.; Giordano, F.; Pellet, N.; Jacopin, G.; Friend, R. H.; Zakeeruddin, S. M.; Grätzel, M. Intrinsic and Extrinsic Stability of Formamidinium Lead Bromide Perovskite Solar Cells Yielding High Photovoltage. *Nano Lett.* **2016**, *16*, 7155−7162.

(17) Arora, N.; Orlandi, S.; Dar, M. I.; Aghazada, S.; Jacopin, G.; Cavazzini, M.; Mosconi, E.; Gratia, P.; De Angelis, F.; Pozzi, G.; et al. High Open-Circuit Voltage: Fabrication of Formamidinium Lead Bromide Perovskite Solar Cells Using Fluorene−Dithiophene Derivatives as Hole-Transporting Materials. *ACS Energy Lett.* **2016**, *1*, 107−112.

(18) Das, J.; Subbiah, A. S.; Mahuli, N.; Singh, R.; Sarkar, S. K. One-step Solution-Processed Formamidinium Lead Tribromide Formation for Better Reproducible Planar Perovskite Solar Cells. *Energy Technol.* **2017**, *5*, 1807−1813.

(19) Xu, H.; Liang, Z.; Ye, J.; Xu, S.; Wang, Z.; Zhu, L.; Chen, X.; Xiao, Z.; Pan, X.; Liu, G. Guanidinium-assisted crystallization modulation and reduction of open-circuit voltage deficit for efficient planar $FAPbBr_3$ perovskite solar cells. *Chem. Eng. J.* **2022**, *437*, No. 135181.

(20) Albrecht, S.; Saliba, M.; Correa Baena, J. P.; Lang, F.; Kegelmann, L.; Mews, M.; Steier, L.; Abate, A.; Rappich, J.; Korte, L.; et al. Monolithic perovskite/silicon-heterojunction tandem solar cells processed at low temperature. *Energy Environ. Sci.* **2016**, *9*, 81−88.

(21) Frost, J. M.; Butler, K. T.; Brivio, F.; Hendon, C. H.; van Schilfgaarde, M.; Walsh, A. Atomistic Origins of High-Performance in Hybrid Halide Perovskite Solar Cells. *Nano Lett.* **2014**, *14*, 2584−2590.

(22) Zheng, X.; Chen, B.; Yang, M.; Wu, C.; Orler, B.; Moore, R. B.; Zhu, K.; Priya, S. The Controlling Mechanism for Potential Loss in $CH_3NH_3PbBr_3$ Hybrid Solar Cells. *ACS Energy Lett.* **2016**, *1*, 424−430.

(23) Hanusch, F. C.; Wiesenmayer, E.; Mankel, E.; Binek, A.; Angloher, P.; Fraunhofer, C.; Giesbrecht, N.; Feckl, J. M.; Jaegermann, W.; Johrendt, D.; Bein, T.; Docampo, P. Efficient Planar Heterojunction Perovskite Solar Cells Based on Formamidinium Lead Bromide. *J. Phys. Chem. Lett.* **2014**, *5*, 2791−2795.

(24) Li, S.; Deng, C.; Tao, L.; Lu, Z.; Zhang, W.; Song, W. Crystallization Control and Defect Passivation via a Cross-Linking Additive for High-Performance $FAPbBr_3$ Perovskite Solar Cells. *J. Phys. Chem. C* **2021**, *125*, 12551−12559.

(25) Zhang, Z.; Wang, X.; Chen, Y.; Zheng, Z.; Xu, W.; Liu, W.; Yang, Y.; Zhao, J.; Chen, T.; Zhu, H. Ultrafast self-trapping of photoexcited carriers sets the upper limit on antimony trisulfide photovoltaic devices. *Nat. Commun.* **2019**, *10*, 4540.

(26) Liu, X.; Zhang, Y.; Shi, L.; Liu, Z.; Huang, J.; Yun, J. S.; Zeng, Y.; Pu, A.; Sun, K.; Hamieri, Z.; et al. Exploring Inorganic Binary Alkaline Halide to Passivate Defects in Low-Temperature-Processed

Planar-Structure Hybrid Perovskite Solar Cells. *Adv. Energy Mater.* **2018**, *8*, No. 1800138.
(27) Zhu, P.; Gu, S.; Luo, X.; Gao, Y.; Li, S.; Zhu, J.; Tan, H. Simultaneous Contact and Grain-Boundary Passivation in Planar Perovskite Solar Cells Using SnO_2-KCl Composite Electron Transport Layer. *Adv. Energy Mater.* **2020**, *10*, No. 1903083.
(28) Nair, V. C.; Muthu, C.; Rogach, A. L.; Kohara, R.; Biju, V. Channeling Exciton Migration into Electron Transfer in Formamidinium Lead Bromide Perovskite Nanocrystal/Fullerene Composites. *Angew. Chem., Int. Ed.* **2017**, *56*, 1214−1218.
(29) Tang, X.; Khurana, M.; Rossi, D.; Luo, L.; Akimov, A. V.; Son, D. H. Exciton Photoluminescence of Strongly Quantum-Confined Formamidinium Lead Bromide ($FAPbBr_3$) Quantum Dots. *J. Phys. Chem. C* **2022**, *126*, 18366−18373.
(30) Liu, Y.; Kim, B. J.; Wu, H.; Boschloo, G.; Johansson, E. M. Efficient and Stable $FAPbBr_3$ Perovskite Solar Cells via Interface Modification by a Low-Dimensional Perovskite Layer. *ACS Appl. Energy Mater.* **2021**, *4*, 9276−9282.
(31) Bhatia, H.; Ghosh, B.; Debroye, E. Colloidal $FAPbBr_3$ perovskite nanocrystals for light emission: what's going on? *J. Mater. Chem. C* **2022**, *10*, 13437−13461.
(32) Jana, A.; Mittal, M.; Singla, A.; Sapra, S. Solvent-free, mechanochemical syntheses of bulk trihalide perovskites and their nanoparticles. *Chem. Commun.* **2017**, *53*, 3046−3049.
(33) Hu, C.; Shivarudraiah, S. B.; Sung, H. H. Y.; Williams, I. D.; Halpert, J. E.; Yang, S. Discovery of a New Intermediate Enables One-Step Deposition of High-Quality Perovskite Films via Solvent Engineering. *Sol. RRL* **2021**, *5*, No. 2000712.
(34) Davies, C. L.; Filip, M. R.; Patel, J. B.; Crothers, T. W.; Verdi, C.; Wright, A. D.; Milot, R. L.; Giustino, F.; Johnston, M. B.; Herz, L. M. Bimolecular recombination in methylammonium lead triiodide perovskite is an inverse absorption process. *Nat. Commun.* **2018**, *9*, 293.
(35) Baranowski, M.; Plochocka, P. Excitons in Metal-Halide Perovskites. *Adv. Energy Mater.* **2020**, *10*, No. 1903659.
(36) Jain, M.; Gill, D.; Bhumia, P.; Basera, P.; Bhattacharya, S. Theoretical insights to excitonic effect in lead bromide perovskites. *Appl. Phys. Lett.* **2021**, *118*, No. 192130.
(37) Shi, J.; Li, Y.; Wu, J.; Wu, H.; Luo, Y.; Li, D.; Jasieniak, J. J.; Meng, Q. Clearly Discriminate the Continuum Band and Exciton State of the Hybrid Lead Bromide Perovskite. arXiv:1902.07371. 2023, DOI: 10.1038/s41420-023-01327-y.
(38) Yamada, Y.; Nakamura, T.; Endo, M.; Wakamiya, A.; Kanemitsu, Y. Photocarrier Recombination Dynamics in Perovskite $CH_3NH_3PbI_3$ for Solar Cell Applications. *J. Am. Chem. Soc.* **2014**, *136*, 11610−11613.
(39) Kiligaridis, A.; Frantsuzov, P. A.; Yangui, A.; Seth, S.; Li, J.; An, Q.; Vayzof, Y.; Scheblykin, I. G. Are Shockley-Read-Hall and ABC models valid for lead halide perovskites? *Nat. Commun.* **2021**, *12*, 3329.
(40) Stranks, S. D.; Burlakov, V. M.; Leijtens, T.; Ball, J. M.; Goriely, A.; Snaith, H. J. Recombination Kinetics in Organic-Inorganic Perovskites: Excitons, Free Charge, and Subgap States. *Phys. Rev. Appl.* **2014**, *2*, No. 034007.
(41) Makarov, N. S.; Guo, S.; Isaienko, O.; Liu, W.; Robel, I.; Klimov, V. I. Spectral and Dynamical Properties of Single Excitons, Biexcitons, and Trions in Cesium−Lead-Halide Perovskite Quantum Dots. *Nano Lett.* **2016**, *16*, 2349−2362.
(42) D'Innocenzo, V.; Grancini, G.; Alcocer, M. J. P.; Kandada, A. R. S.; Stranks, S. D.; Lee, M. M.; Lanzani, G.; Snaith, H. J.; Petrozza, A. Excitons Versus Free Charges In Organo-Lead Tri-Halide Perovskites. *Nat. Commun.* **2014**, *5*, 3586.
(43) Droseros, N.; Longo, G.; Brauer, J. C.; Sessolo, M.; Bolink, H. J.; Banerji, N. Origin of the Enhanced Photoluminescence Quantum Yield in MAPbBr3 Perovskite with Reduced Crystal Size. *ACS Energy Lett.* **2018**, *3*, 1458−1466.
(44) Manser, J. S.; Christians, J. A.; Kamat, P. V. Intriguing Optoelectronic Properties of Metal Halide Perovskites. *Chem. Rev.* **2016**, *116*, 12956−13008.
(45) Rossi, F. Coherent Phenomena in Semiconductors. *Semicond. Sci. Technol.* **1998**, *13*, 147.
(46) Li, M.; Begum, R.; Fu, J.; Xu, Q.; Koh, T. M.; Veldhuis, S. A.; Grätzel, M.; Mathews, N.; Mhaisalkar, S.; Sum, T. C. Low threshold and efficient multiple exciton generation in halide perovskite nanocrystals. *Nat. Commun.* **2018**, *9*, 4197.
(47) Rehman, W.; Milot, R. L.; Eperon, G. E.; Wehrenfennig, C.; Boland, J. L.; Snaith, H. J.; Johnston, M. B.; Herz, L. Charge-Carrier Dynamics and Mobilities in Formamidinium Lead Mixed-Halide Perovskites. *Adv. Mater.* **2015**, *27*, 7938−7944.
(48) Ding, C.; Liu, F.; Zhang, Y.; Hirotami, D.; Rin, X.; Hayase, S.; Monemoto, T.; Masuda, T.; Wang, R.; Shen, Q. Photoexcited hot and cold electron and hole dynamics at $FAPbI_3$ perovskite quantum dots/metal oxide heterojunctions used for stable perovskite quantum dot solar cells. *Nano Energy* **2020**, *67*, No. 104267.
(49) Piprek, J. *Semiconductor Optoelectronic Devices: Introduction to Physics and Simulation* 2003.
(50) Jiang, Q.; Zhang, L.; Wang, H.; Yang, X.; Meng, J.; Liu, H.; Yin, Z.; Wu, J.; Zhang, X.; You, J. Enhanced electron extraction using SnO_2 for high-efficiency planar-structure $HC(NH_2)_2PbI_3$-based perovskite solar cells. *Nat. Energy* **2017**, *2*, 16177.
(51) Bu, T.; Li, J.; Zheng, F.; Chen, W.; Wen, X.; Ku, Z.; Peng, Y.; Zhong, J.; Cheng, Y.-B.; Huang, F. Universal passivation strategy to slot-die printed $SnO_2$for hysteresis-free efficient flexible perovskite solar module. *Nat. Commun.* **2018**, *9*, 4609.
(52) Wang, P.; Wang, J.; Zhang, X.; Wang, H.; Cui, X.; Yuan, S.; Lu, H.; Tu, L.; Zhan, Y.; Zheng, L. Boosting the performance of perovskite solar cells through a novel active passivation method. *J. Mater. Chem. A* **2018**, *6*, 15853−15858.
(53) Dagar, J.; Hirselandt, K.; Merdasa, A.; Czudek, A.; Munir, R.; Zu, F.; Koch, N.; Dittrich, T.; Under, E. L. Alkali Salts as Interface Modifiers in n-i-p Hybrid Perovskite Solar Cells. *Sol. RRL* **2019**, *3*, No. 1900088.
(54) Zhu, N.; Qi, Y.; Zhang, Y.; Liu, G.; Wu, C.; Wang, D.; Guo, X.; Luo, W.; Li, X.; Hu, H.; Chen, Z.; Xiao, L.; Qu, B.; et al. High Efficiency (18.53%) of Flexible Perovskite Solar Cells via the Insertion of Potassium Chloride between SnO_2 and $CH_3NH_3PbI_3$ Layers. *ACS Appl. Energy Mater.* **2019**, *2*, 3676−3682.
(55) Kim, S. Y.; Zhang, F.; Tong, J.; Chen, X.; Enkhbayar, E.; Zhu, K.; Kim, J. H. Effects of potassium treatment on SnO_2 electron transport layers for improvements of perovskite solar cells. *Solar Energy* **2022**, *233*, 353−362.
(56) Wu, K.; Chen, J.; Lian, T. Efficient hot-electron transfer by a plasmon-induced interfacial charge-transfer transition. *Science* **2015**, *349*, 632−635.